

Cathode fall voltage of TIG arcs from a non-equilibrium arc model

D. Uhrlandt · M. Baeva · A. V. Pipa · R. Kozakov · G. Gött

Received: 4 January 2014 / Accepted: 8 July 2014 / Published online: 14 August 2014
© The Author(s) 2014. This article is published with open access at Springerlink.com

Abstract This work presents modelling results concerning a tungsten inert gas (TIG) welding arc. The model provides a consistent description of the free burning arc, the arc attachment and the electrodes. Thermal and chemical non-equilibrium is considered in the whole arc area, and a detailed model of the cathode space-charge sheath is included. The mechanisms in the cathode pre-sheath are treated in the framework of a non-equilibrium approach which is based on a two-fluid description of electrons and heavy particles and a simplified plasma chemistry of argon. A consistent determination of the electrode fall voltages and temperature distributions is achieved. The model is applied to arcs in pure argon at currents up to 250 A, whereby welding of a workpiece made of mild steel with a fixed burner is considered. Arc voltages in the range from 12 to 17 V are obtained at 50 at 250 A, respectively. The space-charge sheath voltage is found to be about 7 V and almost independent of the current. The corresponding temperatures of the cathode tip are in the range from 3,000 K to about 3,800 K. The results obtained are in a good agreement with measurements.

Keywords Tungsten · Inert gases · Welding · Computation · Arc welding · Simulating · Cathodes · Temperature

1 Introduction

Tungsten inert gas (TIG) welding is widely used in metal working industry. It is a quite stable process suitable for

low-alloy steel and stainless steel as well as aluminium or titanium. The argon-shielding gas ensures high purity of the process.

At the same time, the TIG process has been widely used as a standard example for modelling of free burning arcs. That is because of two facts simplifying the modelling: the use of pure argon at atmospheric pressure and the non-consumable and non-refractory tungsten cathode, which can be described neglecting geometric changes. In addition, a simplified rotationally symmetric configuration of a TIG process with a fixed burner perpendicular to a flat work piece is considered in the most cases.

There is a long history of modelling TIG arcs with a large variety of different model assumptions. Earlier models consider only the arc column as plasma in local thermodynamic equilibrium (LTE) (see, e.g. [1]). Other modelling works focus on the energy transfer to the anode (the work piece) and determination of the anode temperature profile and more recently also the weld pool behaviour (see, e.g. [2, 3] and references therein). Some other models consider in particular the interaction of the arc with the tungsten cathode determining the cathode temperature distribution (see, e.g. [4]) and the important impact of different emitter materials [5]. However, the interaction between arc and electrode surfaces has been strongly simplified in most of the models avoiding the detailed description of the arc sheath region with its strong departures from LTE. For that reason, the total voltage drop being measured in experiments has not been confirmed by modelling [4].

The total voltage drop includes beside the voltage over the arc column also the cathode and anode fall voltages and voltage drops in the electrodes. For a proper description of the electrode fall voltage, the voltage drops over the space-charge sheath and the ionisation sheath have to be considered. Measurements for tungsten [6] and fusible electrodes [7] justify the importance of the electrode fall voltages but show

Doc. IIW-2500, recommended for publication by Study Group SG-212 "The Physics of Welding"

D. Uhrlandt (✉) · M. Baeva · A. V. Pipa · R. Kozakov · G. Gött
Leibniz Institute for Plasma Science and Technology,
17489 Greifswald, Germany
e-mail: uhrlandt@inp-greifswald.de

also the difficulties and limited precision of an experimental determination.

One option for the description of the sheath voltages is the coupling of an LTE arc column model with a separate non-linear sheath model including ionisation and space-charge sheath (see, e.g. [8]). The ionisation sheath model has to take into account departures from thermal and ionisation equilibrium in this plasma region. Also, the consistent coupling with the heat balance of the electrodes is mandatory. An example of such a model for a cylindrical tungsten cathode focusing on the non-equilibrium transport properties in the sheath regions is given in [9]. However, the transition region from the ionisation sheath to the arc column can be in addition affected by unequal electron and heavy particle temperature. This fact can be considered in a proper way replacing the LTE arc model by a two-temperature plasma model. This option has been applied recently to the description of a TIG arc including the cathode fall and the tungsten cathode temperature [10]. The results are in a good agreement with the measurements. Anode voltage drop and voltage drops inside the electrodes were not included in this model and can be neglected in a first approximation. The work illustrates in addition that LTE arc models overestimate the arc column voltage. They are not able to describe the dependence total voltage — arc current even if a constant cathode fall voltage is assumed and added to the arc column voltage.

Another option is to employ a non-equilibrium model of the arc core together with the ionisation layer avoiding in that way any assumptions of thermal, chemical and ionisation equilibrium. Hence, a complementally treatment of the space-charge sheath is needed only. Such a model has been developed recently for a simplified TIG process (tungsten thermionic cathode and cooled copper plate as anode) and validated by spectroscopic measurements [11]. The model has been also applied to the configuration of the TIG arc in [10], and the results in particular for the voltage drops have been compared for varying currents [12]. A general agreement of the results has been found, but the non-equilibrium model provides an even more precise estimation of the measured voltages.

The aim of this paper is the application of the model proposed in [11] to a more realistic TIG process and the determination of the total voltage drops as well as the tungsten cathode temperature distribution for different arc currents and electrode distances. The considered setup of the TIG experiment is described in Section 2 together with diagnostic methods. The main features of the model are given in Section 3. Section 4 includes the results, the comparison with measurements and a discussion. Conclusions and outlook are given in Section 5.

2 Setup and measurements

For the TIG experiment, a commercial burner having a rod cathode with a diameter of 3.2 mm sharpened by an angle of

30° and a nozzle with an inner diameter of 11 mm has been used. The cathode material was tungsten with 5 % oxide admixture as a replacement of thorium oxide. The burner was placed perpendicular to the work piece in order to provide a rotationally symmetric construction. The distance between the electrode tip and nozzle edge has been fixed at 3.5 mm. Ten-millimeter-thick plates of mild steel (S235) served as a work piece. Welding experiments have been done with a fixed burner and work piece, always the same flow rate of 12 standard litre per minute (slm) of pure argon as shielding gas, distances of 6, 8 and 10 mm between the electrode tip and work piece and DC currents of 50, 100, 150, 200 and 250 A employing the tungsten electrode as a cathode. The TIG arc current has been switched on for about 20 s to ensure the almost-established steady-state conditions of the process including the melting of the work piece.

The voltage has been measured between the work piece and a contact at the rod electrode with a differential probe. The arc current has been measured by a Hall probe. The arc has been observed from the sight (perpendicular to the arc axis) with a high-speed camera using a framing rate of 50/s and acquisition times between 10 and 30 μ s. The camera was equipped with a specified optical setup which allows the simultaneous recording of two images of the arc with two different filters. Metal interference filters with band widths of few nanometres and maximum selectivity appropriate to an argon atom line in the near infrared region and near an argon ion line in the blue visible range have been applied.

3 Non-equilibrium model

The model comprises a consistently coupled description of the relevant gas volume including the arc column region and the electrode sheath regions, a main part of the tungsten cathode, a part of the steel work piece over the whole thickness, and a specific model of the space-charge sheath and the relevant processes at the electrode surfaces. The model has been already described in detail in [11] and shall be briefly explained in what follows from the point of view of the basic physical background and the corresponding boundary conditions.

The solution area is illustrated in Fig. 1. A rotationally symmetric setup is considered including parts of the gas volume, the electrodes and the nozzle. Notice that a small flat area (0.2 mm in radius) at the tip of the tungsten electrode has been introduced in order to represent the realistic geometry after some time of operation. However, the distance between the cathode tip and the work piece as used in this paper corresponds to the distance to the fresh sharpened cathode, i.e. without the flattened part. The solution area is discretized by a non-equidistant-structured grid in the volume of a 10° slice corresponding to the assumed symmetry.

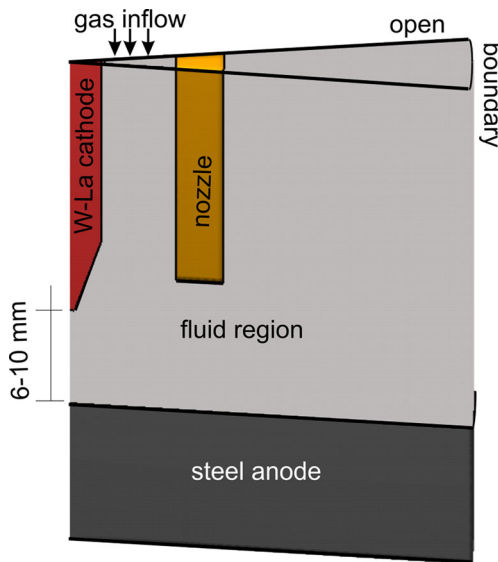


Fig. 1 Solution area for the model of the TIG process

The heat balance and current conservation equations are solved in the parts of the electrodes considering the temperature dependence of the thermal and electrical conductivity of the materials. Fixed temperatures of 700 K at the lower side of the work piece and 300 K at the upper side of the cathode serve as boundary conditions of the heat balances together

$$\frac{\partial}{\partial t}(\rho c_p T_g) + \nabla \cdot (\rho c_p T_g \vec{v}) = \nabla \cdot \left(\lambda \nabla T_g + \sum_k \vec{J}_k Y_k c_{pk} \nabla T_g \right) + \frac{\partial p}{\partial t} + \hat{\tau} : \vec{v} + Q_{in} + Q_{nn} + Q^{el} \frac{3}{2} \frac{\partial}{\partial t} (n_e k_B T_e) + \nabla \cdot \left(\frac{5}{2} k_B T_e \vec{T}_e - \lambda_e \nabla T_e \right) = \vec{j} \cdot \vec{E} - Q^{inel} - Q_{rad} - Q^{el}$$

for heavy particles and electrons and the ideal gas law. Here, ρ , \vec{v} and p are the mean mass density, velocity and pressure; $\hat{\tau}$ is the viscous stress tensor; \vec{j} , \vec{E} and \vec{B} are the electric current density, electric and the self-induced magnetic field; and n_e , \vec{J}_k and \vec{T}_e are the electron density, the heavy particle flux density and the electron flux density, respectively. λ and λ_e denote the thermal conductivities of heavy particles and electrons; c_p and c_{pk} represent the specific heat of the mixture and the individual components. The energy density due to elastic electron collisions with heavy particles Q^{el} serves as the main coupling term of both energy balances. Furthermore, energy gain/loss due to ion-neutral (Q_{in}), neutral-neutral (Q_{nn}), inelastic electron-neutral collisions (Q^{inel}) and radiation (see details in [11]) is accounted for. The Ohmic heating $\vec{j} \cdot \vec{E}$ is the main gain term in the electron energy balance. The Lorentz force ($\vec{j} \times \vec{B}$) is considered in the momentum balance. Transport properties (heat conductivities of electrons and heavy particles,

with net heat flux densities from the plasma (see below). Because the weld pool description is out of the scope of this study, the flow in the melted part of the work piece has not been taken into account.

The magneto-hydrodynamic description of the TIG process includes the solution of an equation for the magnetic vector potential and the magnetic field of the arc current in the whole solution area as well as the current conservation equation in the gas volume. Zero potential has been considered at the lower side of the work piece, and a uniform current density corresponding to the given current and cathode cross section is set at the upper boundary of the cathode. Zero vector potential has been set at the outer boundary of the cylindrical solution area, zero gradient at the borders perpendicular to the axis.

Special effort has been spent to develop a description of the arc area avoiding assumptions of thermal, chemical and ionisation equilibrium. Therefore, separate energy balance equations are solved to determine the electron temperature (T_e) and the temperature of heavy particles (T_g). The continuity and momentum balance equations of the flow

$$\frac{\partial \rho}{\partial t} + \nabla \cdot (\rho \vec{v}) = 0 - \frac{\partial (\rho \vec{v})}{\partial t} + (\rho \vec{v} \cdot \nabla) \vec{v} = -\nabla p + \nabla \cdot \hat{\tau} + \vec{j} \times \vec{B}$$

are solved along with the energy balances

electrical conductivity) have been determined for two-temperature plasma conditions.

A constant flow velocity corresponding to the given shielding gas flow (12 slm pure argon) is applied at the border between cathode and inner nozzle wall. The pressure (1 bar) is fixed at the open borders of the gas volume.

The contributions of the relevant collision processes are treated separately by calculating their collision rates using cross sections for argon. Therefore, a simplified plasma chemistry model for argon has been adapted including implicitly the lowest excited levels (four 4 s states) of argon. The mass fraction Y_k of argon ions is determined by solving the mass fraction conservation equation

$$\frac{\partial}{\partial t}(\rho Y_k) + \nabla \cdot (\rho \vec{v} Y_k) = \nabla \cdot \vec{J}_k + S_k$$

where S_k represents the production/loss of argon ions due to ionisation, three-body recombination and radiative

recombination. The diffusive flux density, \vec{J}_k , in this equation contains an effective diffusion coefficient calculated from binary diffusion coefficients and terms accounting for thermal and pressure diffusion and the drift in the electric field. The collision processes are described by their individual cross sections and rates based on the assumption of prompt ionisation. Argon molecule reactions and the chemistry of ions of higher charge state have been neglected for simplicity reasons. Quasi-neutrality in the whole gas volume is assumed in order to obtain the electron density. Recombination at the solid walls and vanishing mass fractions at the open boundaries serve as boundary conditions.

Special effort has also been spent to describe the relevant processes in the arc attachment area — the space-charge sheath and the processes at the electrode surfaces. At the cathode surface, the thermionic emission of electrons is described by the Richardson equation including Schottky correction of the work function of the cathode material (tungsten with oxide admixture). The total electric current density is expressed as the sum of the densities of the emission current, the ion current corresponding to the Bohm flux, and the electron back flux dependent on the electron density at the sheath edge and the voltage drop over the space-charge sheath. The latter is calculated from the balance of energy fluxes at the sheath edge, i. e. between the arc plasma (the non-equilibrium pre-sheath) and the space-charge sheath according to [13]. Then, the net heat flux density onto the cathode surface is calculated from the balance of all contributions from particle fluxes and the radiation of the cathode surface. This heat flux density is used as the boundary condition of the cathode heat balance.

At the anode surface, the electron emission is neglected because of the much lower surface temperature. Metal evaporation is also neglected for simplicity reasons. The net heat flux density is expressed by the leading term, the electron current density from the plasma times the recombination energy, reduced by the surface radiation term.

The electron fluxes to the electrode surfaces as well as to other walls corresponding to the wall recombination are used to determine the respective energy fluxes as boundary conditions for the electron energy balance.

The initial conditions of the simulation are an electron temperature of 1 eV, a heavy particle temperature of 1,000 K, an ionisation degree of 1 % and a flow velocity of 1 m/s in axial direction. Once ignited, the arc is further sustained self-consistently due to the flow, the electromagnetic field, the power supply and the boundary conditions. The system of equations is solved under steady-state conditions using the commercial code CFD-ACE+ [14] based on finite-volume discretisation.

4 Results and discussion

Experiments and simulations have been performed for distances of 6, 8 and 10 mm between the cathode tip and work piece. Lower distances have been omitted here to study mainly the arc attachment at the cathode without disturbing influences of the anode, the metal evaporation among others. For each inter-electrode distance, arc currents from 50 up to 250 A have been considered. The profiles of the electron and heavy-particle temperatures resulting from the model are shown in Fig. 2 for the lowest and largest values of the considered distances and currents. A lower current leads to a larger width of the hot region and lower temperature maximum. There is a difference of about 6,000 K in the maxima between arc current 50 and 250 A. At higher currents, the hot region is more focussed near the tip of the cathode. While the heavy particle temperature drops down towards the electrode surfaces and the arc surrounding, the electron temperature shows a much lower decrease or even an increase near the cathode tip. The distance has only small influence on the general arc structure. Notice that the maximum temperatures are rather low in comparison with other model results (e.g. for 200 A in [15]). Results in [16] for 150 A are rather comparable. As pointed out in [17], higher temperatures near the cathode result from the model if the arc cathode attachment (the application range of the sheath model as explained in Section 3) is restricted to a proper part of the cathode. However, to study different arc currents with a physically consistent model and without further input from the experiment, a common size of the attachment area has been used for all current values in the present work. The overcoming of this limitation is aspired in forthcoming improvements of the model.

Figure 3 shows the simulation results for the temperature distribution in the cathode for the examples considered in Fig. 2. At arc current of 250 A, the maximum temperature at the cathode tip is by more than 700 K higher than at 50 A. The electrode distance is of less impact on the cathode temperature. However, the temperature in the upper part of the sharpened region of the cathode is a little higher in case c in Fig. 3 (10 mm and 50 A) in comparison with case a (6 mm and 50 A) in spite of the small changes in the heavy particle temperature near the cathode surface. These results are in good agreement with pyrometric measurements [18] which are reported, however, for slightly different parameters (tungsten electrode with 2 % ThO₂ of 2.4-mm diameter and a cone tip of 68°). Tip temperatures of about 3,700 K are obtained for currents above 130 A (including 200 A). The tip temperature decreases to about 3,000 K at 50 A and 2,900 K at 30 A [18].

High-speed images of the arc recorded from the side in the corresponding experiment are shown in Figs. 4 and 5. The comparison of the radiation in the small ranges of an argon atom line and an argon ion is given in Fig. 4 for the case of a high current of 250 A. The radiation profile in part a (argon

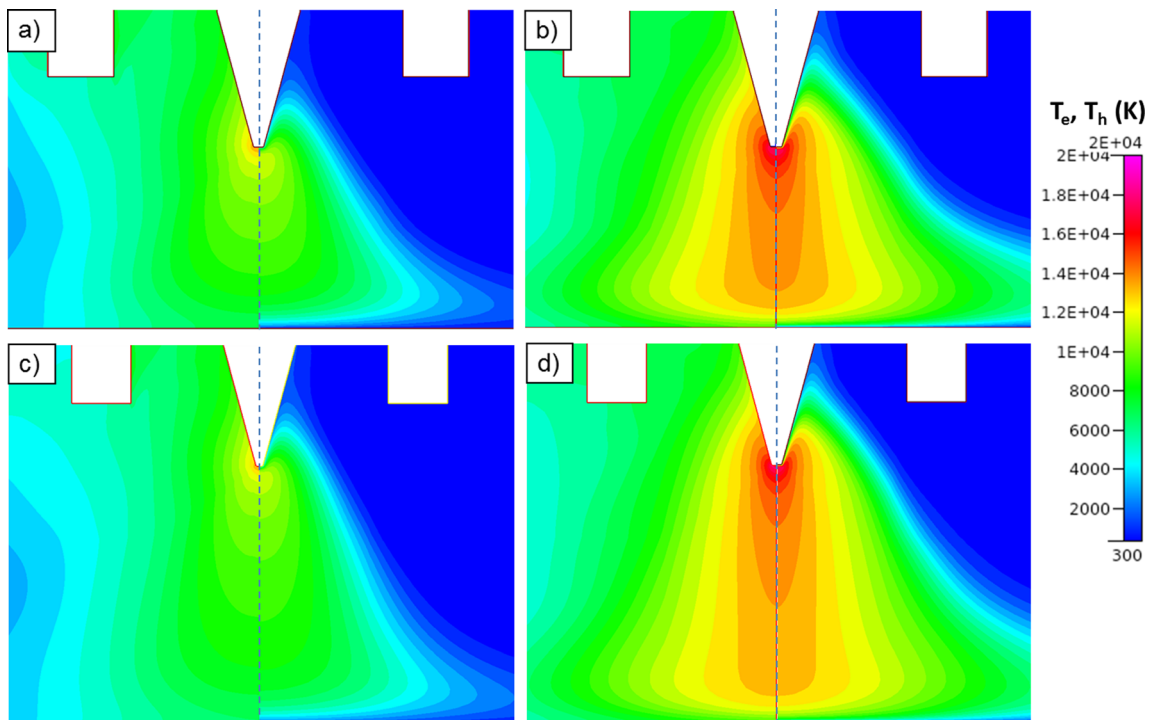


Fig. 2 2D-profiles of the electron temperature T_e (left side in each picture) and heavy-particle temperature T_h (right side in each picture) in the arc calculated **a** for the electrode distance 6 mm and the current 50 A, **b** 6 mm and 250 A, **c** 10 mm and 50 A and **d** 10 mm and 250 A

atom line) looks quite similar to the calculated profile of the temperature profile given in Fig. 2d. There is one important exception, the darker region in the surrounding of the cathode tip. In the same region, a strong radiation of the ion line can be seen in Fig. 4b. This finding coincides with the high temperatures up to 18,000 K calculated in this region (compare

Fig 2d) where on the one hand, the ionisation degree increases and the temperature is high enough for the excitation of the argon ion. On the other hand, the temperature is higher than the norm maximum of the corresponding argon atom line (around 15,000 K). This leads to the decrease of the atom radiation near the cathode tip.

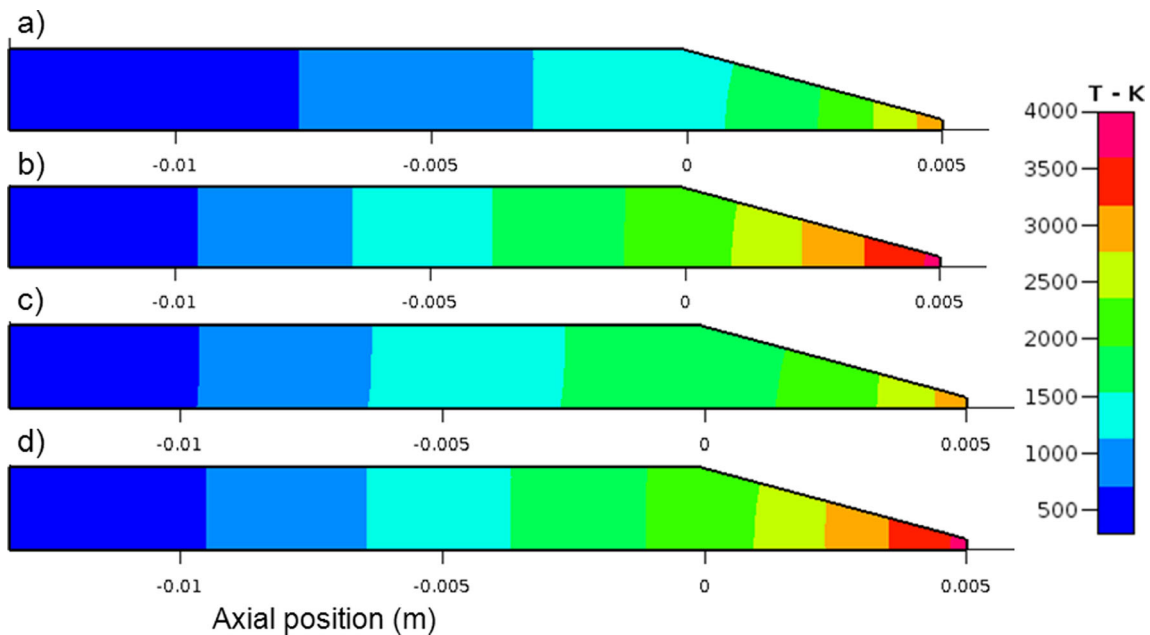
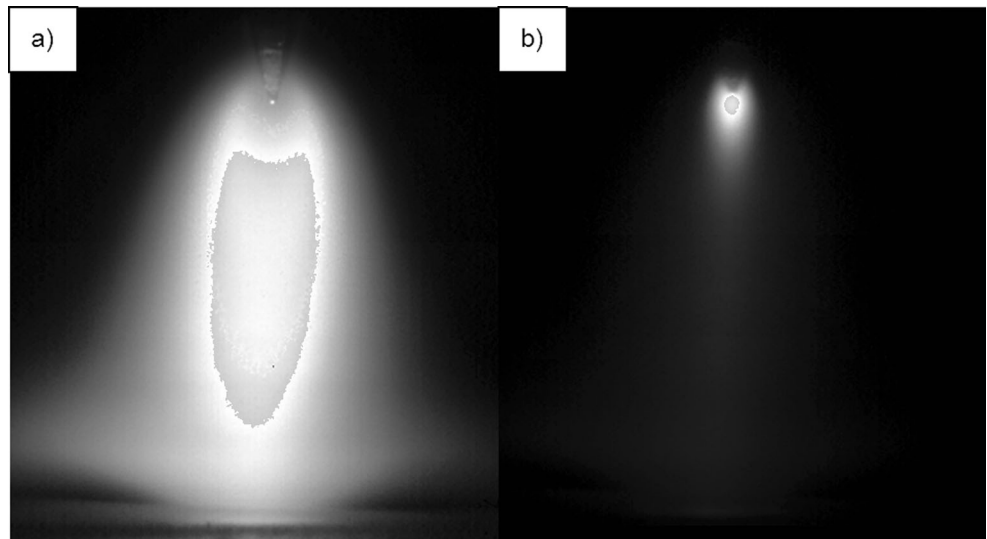


Fig. 3 2D-profiles of the calculated cathode temperature T_c for the cases **a** to **d** as in Fig. 2

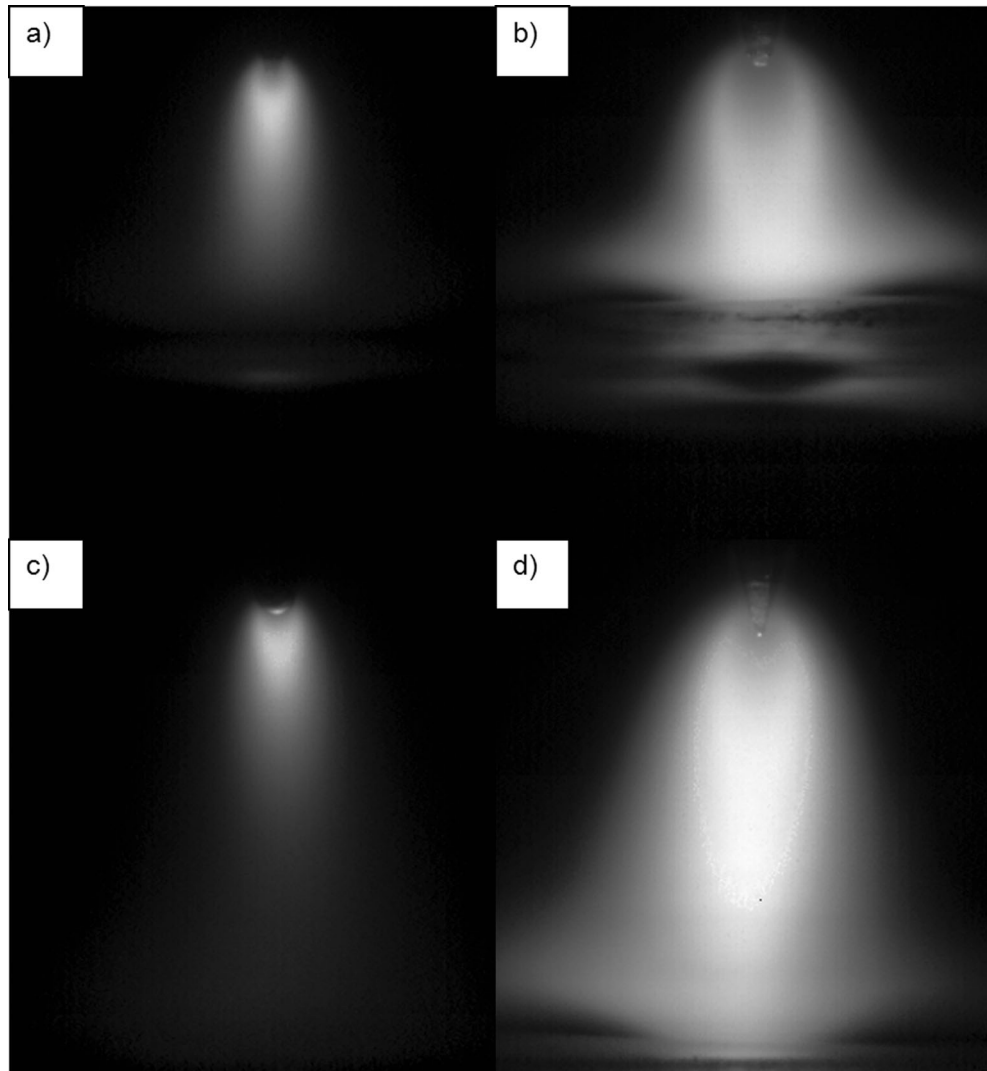
Fig. 4 High-speed images of the arc obtained with spectral filters **a** for an Ar atom line and **b** for and Ar ion line for the electrode distance of 10 mm and the current 250 A



In Fig. 5, the high-speed images in the spectral range of the argon atom line are compared for the four limiting cases

considered already in Fig. 2. Obviously, the radiation is much more intensive and the arc profile is broader in the cases for

Fig. 5 High-speed images of the arc obtained with spectral filter for an Ar atom line for the cases **a** to **d** as in Fig. 2



the current 250 A compared with 50 A. Notice that the image brightness of parts a and c has been increased manually after calibration of all images to improve the visibility of the arc structure in the cases for the low current 50 A. Comparing the images for different arc length and the same current, the radiation profiles in the upper part of the arc are quite similar in each case. The structure in the lower part corresponds to the elongation of the arc. Considering the exception of the lower atomic line radiation near the cathode tip, all four images reflect well the differences in the arc structure found in the calculated temperature profiles of the heavy particles in Fig. 2. The occurrence of the local minimum in the radiation near the cathode tip in the cases of 250 A (Fig. 5b, d) as well as the

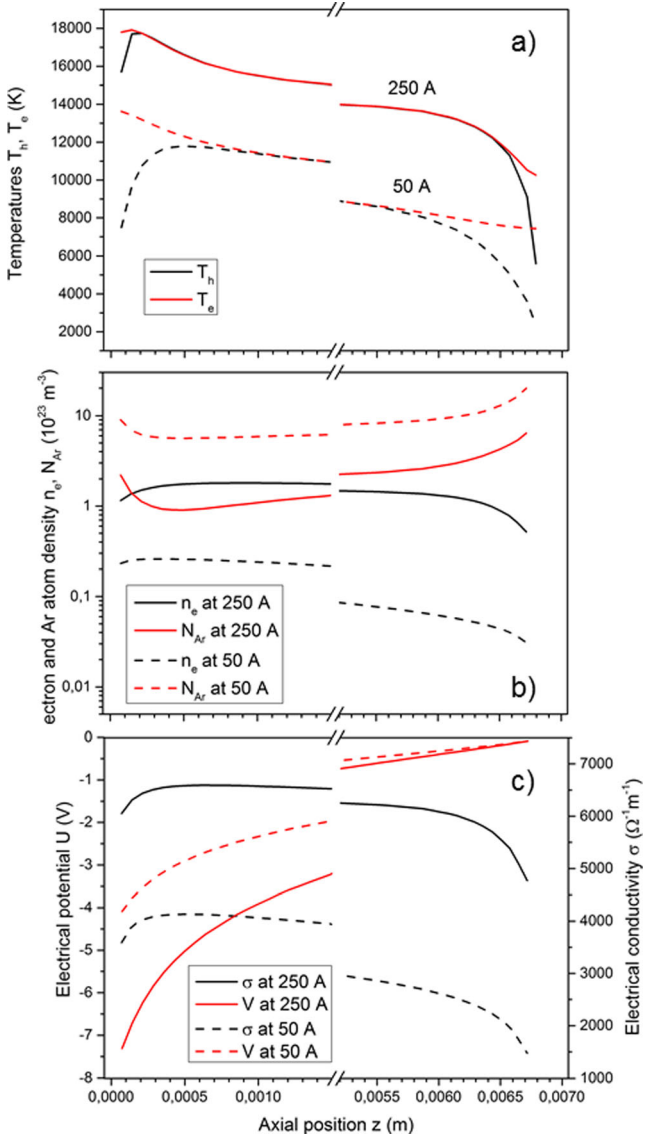


Fig. 6 Examples of the axial courses **a** of the electron temperature T_e and the heavy particle temperature T_h , **b** the electron density n_e and the Ar atom density N_{Ar} and **c** of the electrical conductivity σ and potential U in the arc axis for the electrode distance 10 mm and the current 50 and 250 A

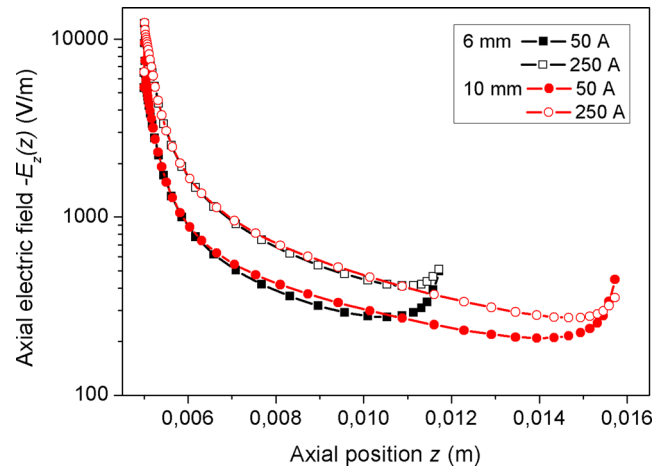


Fig. 7 Axial electric field at the arc axis for the four cases considered in Fig. 2

absence of such a minimum at 50 A (Fig. 5a and b) confirms the range of temperatures obtained from the model.

A more detailed validation of the model results for the arc properties with spectroscopic measurements was the subject of a recent work [10].

In what follows, the results for temperatures, densities and electrical quantities along the arc axis are in the focus. Figure 6 shows axial courses of these quantities for two cases: 6 mm arc length, 50 and 250 A. A range in the middle of the arc is omitted to provide a more detailed comparison in the ranges near the electrodes. As expected, the quantities differ considerably for the two different currents. Most part of the arc is in thermal equilibrium at least in the arc centre. Near both electrodes, the heavy particle temperature approaches the electrode surface temperature whereas the electron temperature remains well above and ensures a high electrical conductivity near the surfaces. These regions of pronounced deviations between both temperatures can be identified with the pre-sheath regions (or ionisation sheath regions). The electron

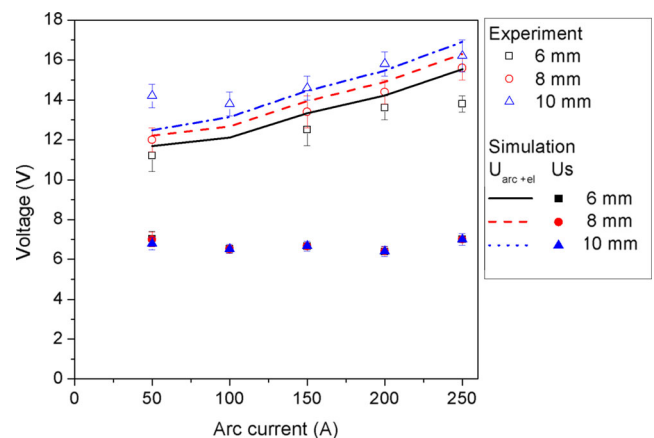


Fig. 8 Measurements of the arc voltage and comparison with the simulation results (total voltage U_{arc+el} and voltage drop over the space-charge sheath U_s) for the three electrode distances as function of the current

density (equal to the Ar^+ ion density in the model) and the electrical conductivity show little decrease near the electrodes whereas the Ar atom density slightly increases because of the temperature decrease. An ionisation degree lower than 20 % is obtained in case of the low current 50 A.

The potential course with large gradients near the cathode surface leads to a voltage drop of about 7.5 V in the case of 250 A and about 4 V for 50 A.

A more detailed insight into the structure of the electric potential can be provided by the model results for the axial electric field strength. Results for the four examples considered in the figures before are given in Fig. 7. A semi-logarithmic scale has been chosen to illustrate the large changes in the axial field. As it can be seen in Fig. 7, very high field values are achieved when approaching the cathode tip. There is also a distinct increase when approaching the anode (the work piece). The high values near the electrodes are very similar for different currents and electrode distances and can be indicated as the electric field values at each edge of the pre-sheath and the space-charge sheath at cathode and anode, respectively. Away from the electrodes, there is a continuous decrease of the axial field values with increasing distance from the cathode. The higher current leads to higher values in the arc column. The values for the same current are very similar compared at the same distance from the cathode. For the longer arc, the axial field values in the lower arc part correspond well to an extrapolation of the course in the upper part.

An important result of the model is the total voltage drop between work piece and the upper border of the cathode. This voltage $U_{\text{arc+el}}$ is the sum of the voltage drop over the arc column including the pre-sheath regions, the voltage fall in the space-charge sheath (considered at the cathode) and the voltage drop over the electrodes. Notice that the space-charge sheath at the anode is neglected in the model. The total voltage drop can be well compared with measured voltages between contacts at the work piece and the tungsten rod cathode. The comparison of these calculated and measured voltages is shown in Fig. 8. The error bars of the measured voltages correspond to the remaining variation in time and in different experiments with the same measured current. The simulation results coincide with the measurements within their accuracy limits in most of the cases.

Above 100 A, there is an almost linear increase of the voltage with the current. Going from 50 to 100 A, the total voltage shows only small changes or obeys even a minimum at 100 A. This result is in agreement with recent findings for other cathode geometries [12, 17]. Except for the current 50 A, the voltage drop changes by about 0.7 V when changing the electrode distance by 1 mm. This relatively small value corresponds qualitatively to the range of the axial field strength from 0.2 to 1 V/mm in the main parts of the arc, as illustrated in Fig. 7. The voltage drop U_S over the space-charge sheath at the cathode is around 7 V and almost independent of current and electrode

distance. The error bars indicate small changes of this voltage along the cathode tip. The voltage drop over the rod cathode is also included but not separately plotted in Fig. 8. The model yields values between about 0.2 V at a current of 50 A and 0.5 V at a current of 250 A. The main contribution to this voltage drop results from the hot part (above 2,000 K) of the cathode.

5 Conclusion

The non-equilibrium arc model including the description of the cathode space-charge sheath is capable of predicting the arc voltage of a TIG process for different currents and electrode distances. The results, in particular for the total voltage drops and the cathode tip temperature, are in a good agreement with own measurements and literature data. The specific model allows the separate analysis of the leading voltage drops in the TIG process, in particular the voltage drops over the cathode space-charge sheath, the pre-sheath regions and the arc column.

The following conclusions can be drawn from the results of the simulation and measurements:

- (a) The voltage drop over the space-charge sheath at the cathode is almost independent of current and electrode distance and contributes with up to 50 % to the total voltage drop.
- (b) The axial electric field values at the edges of the pre-sheath regions are also almost independent of current and electrode distance.
- (c) The axial electric field in the arc column depends on the arc current and decreases with increasing distance from the cathode. For longer arcs, the course of the axial electric field in the arc column (without sheath regions) corresponds approximately to the extrapolation of that in a shorter arc.

Investigations with the model have been done so far for specific tungsten cathodes and simplified boundary conditions with respect to the cooling of the cathode. Next investigations will be aimed at analysing the influence of the cathode shape and the cathode cooling on the arc structure and the current-voltage characteristics.

Acknowledgments This work was supported by the German Science foundation (DFG) under grant UH 106/6-1.

Open Access This article is distributed under the terms of the Creative Commons Attribution License which permits any use, distribution, and reproduction in any medium, provided the original author(s) and the source are credited.

References

1. Ducharme R, Kapadia P, Dowden J, Thornton M, Richardson I (1995) A mathematical model of the arc in electric arc welding including shielding gas flow and cathode spot location. *J Phys D: Appl Phys* 28:1840–1850

2. Haidar J (1998) A theoretical model for gas metal arc welding and gas tungsten arc welding. *J Appl Phys* 84:3518–3529
3. Tanaka M, Lowke JJ (2007) Predictions of weld pool profiles using plasma physics. *J Phys D: Appl Phys* 40:R1–R23
4. Bini R, Monno M, Boulos MI (2006) Numerical and experimental study of transferred arcs in argon. *J Phys D: Appl Phys* 39:3253–3266
5. Yamamoto K, Tashiro S, Tanaka M (2009) Numerical analysis of current attachment at thermionic cathode for gas tungsten arc at atmospheric pressure *Transactions of JWRI* 38:1–5
6. Luhmann J, Lichtenberg S, Langenscheidt O, Benilov MS, Mentel J (2002) Determination of HID electrode falls in a model lamp II: Langmuir-probe measurements. *J Phys D: Appl Phys* 35:1631–1638
7. Hajosy R, Morva I (1994) Cathode and anode falls of arcs with fusible electrodes. *J Phys D: Appl Phys* 27:2095–2101
8. Benilov MS (2008) Understanding and modelling plasma–electrode interaction in high-pressure arc discharges: a review. *J Phys D: Appl Phys* 41:144001
9. Gonzalez JJ, Cayla F, Freton P, Teulet P (2009) Two-dimensional self-consistent modelling of the arc/cathode interaction. *J Phys D: Appl Phys* 42:145204
10. Benilov MS, Benilova LG, Li H-P, Wu G-Q (2012) Sheath and arc-column voltages in high-pressure arc discharges. *J Phys D: Appl Phys* 45:355201
11. Baeva M, Kozakov R, Gorchakov S, Uhrlandt D (2012) Two-temperature chemically non-equilibrium modelling of transferred arcs. *Plasma Sources Sci Technol* 21:055027
12. Baeva M, Uhrlandt D, Benilov MS, Cuhna MD (2013) Comparing two non-equilibrium approaches to modelling of a free-burning arc. *Plasma Sources Sci Technol* 22:065017
13. Benilov MS, Marotta A (1995) A model of the cathode region of atmospheric pressure arcs. *J Phys D: Appl Phys* 28:1869
14. CFD-ACE+, ESI CFD Inc., Version 2010
15. Wu CS, Ushio M, Tanaka (1997) Analysis of the TIG welding arc behavior. *Comp Mat Sci* 7:308–314
16. Murphy AB, Tanaka M, Tashiro S, Lowke JJ (2009) A computational investigation of the effectiveness of different shielding gas mixtures for arc welding. *J Phys D: Appl Phys* 42:115205
17. Baeva M, Gorchakov S, Kozakov R, Uhrlandt D, Schoenemann T (2013) Non-equilibrium modelling of the electrical characteristics of a free-burning arc. *High Voltage Engineering* 39:2159–2165
18. Sillero JA, Ortega D, Munoz-Serrano E, Casado E (2010) An experimental study of thoriated tungsten cathodes operating at different current intensities in an atmospheric-pressure plasma torch. *J Phys D: Appl Phys* 45:185204